

Negative photoconductivity and hot-carrier bolometric detection of terahertz radiation in graphene-phosphorene hybrid structures

V. Ryzhii^{1,2,3,4*}, M. Ryzhii⁵, D. S. Ponomarev^{2,3}, V. G. Leiman³, V. Mitin^{1,6}, M. S. Shur^{7,8}, and T. Otsuji¹

¹ *Research Institute of Electrical Communication,
Tohoku University, Sendai 980-8577, Japan*

² *Institute of Ultra High Frequency Semiconductor Electronics of RAS,
Moscow 117105, Russia*

³ *Center of Photonics and Two-Dimensional Materials,
Moscow Institute of Physics and Technology,
Dolgoprudny 141700, Russia*

⁴ *Center for Photonics and Infrared Engineering,
Bauman Moscow State Technical University,
Moscow 111005, Russia*

⁵ *Department of Computer Science and Engineering,
University of Aizu,
Aizu-Wakamatsu 965-8580, Japan*

⁶ *Department of Electrical Engineering,
University at Buffalo, Buffalo, New York 1460-192*

⁷ *Department of Electrical, Computer,
and Systems Engineering and Department of Physics,
Applied Physics, and Astronomy,
Rensselaer Polytechnic Institute,
Troy, New York 12180, USA*

⁸ *Electronics of the Future,
Inc., Vienna, VA 22181, USA*

We consider the effect of terahertz (THz) radiation on the conductivity of the ungated and gated graphene (G)-phosphorene (P) hybrid structures and propose and evaluated the hot-carrier uncooled bolometric photodetectors based on the GP-lateral diodes (GP-LDs) and GP-field-effect transistors (GP-FETs) with the GP channel. The operation of the GP-LDs and GP-FET photodetectors is associated with the carrier heating by the incident radiation absorbed in the G-layer due to the intraband transitions. The carrier heating leads to the relocation of a significant fraction of the carriers into the P-layer. Due to a relatively low mobility of the carriers in the P-layer, their main role is associated with a substantial reinforcement of the scattering of the carriers. The GP-FET bolometric photodetector characteristics are effectively controlled by the gate voltage. A strong negative conductivity of the GP-channel can provide much higher responsivity of the THz hot-carriers GP-LD and GP-FET bolometric photodetectors in comparison with the bolometers with solely the G-channels.

I. INTRODUCTION

Unique energy spectra, of graphene (G) [1] and a few-layer Black Phosphorus layer or phosphorene (P) [2], their optical and electric properties, and recent advances in technology open remarkable prospects for the creation of novel devices using G-layers [3–6], the P-layers [2, 7–10], and different hybrid structures including the G-P hybrid structures [11–13]. In particular, the GP hybrid systems can be used for the improvement of various devices. The possibility of the layer-dependent alignment work function control [2, 14] provides substantial flexibility in the device design. In this paper, we propose and evaluate the detector of the terahertz (THz) radiation based on a lateral diode (LD) and a field-effect transistor (FET) with the GP channel, GP-LD and GP-FET, respectively. The operation of the GP-LD and GP-FET photodetectors with the GP-channel is associated with

the carrier heating by the incident radiation absorbed in the G-layer leading to a variation of the channel conductivity [15, 16]. This principle is used in the hot-carrier bolometers based on the G-channel exhibiting the negative or positive photoconductivity (see, for example [17–21] and references therein). However, a major disadvantage of using G-layers in the bolometric photodetectors is that the conductivity of pristine G-layers is weakly dependent on the carrier temperature. This can be overcome by the introduction of the barrier regions (by partitioning of the channel into nanoribbons in which the energy gap is opened [17] or using disordered G-layers [20]). In the G-P bolometers under consideration, the carrier heating caused by the absorbed radiation leads to the transfer of a significant portion of the carriers into the P-layer. This results in a decrease of the density of the highly mobile carriers in the G-layer and in a reinforcement of the scattering of these carriers on the carriers residing in the P-layer. Due to a high effective mass of

the carriers in the P-layer and, hence, a relatively low mobility, their main role is associated with a substantial reinforcement of the scattering of the carriers in the G-layer. As a result, the conductivity of the GP-channel can markedly drop with the carrier heating. We demonstrate that the effect of the negative THz photoconductivity in the G-P channels can be much stronger than that for the G-channels, particularly at room temperature. Therefore, the GP-LDs and GP-FETs could effectively operate as the uncooled hot-carrier THz bolometers with an elevated responsivity.

II. MODEL

Figure 1 demonstrates a schematic view of the ungated and gated G-P structures (i.e., a GP-LD and a GP-FET with the GP-channels). It is assumed that the P-layer consisting of a few atomic layers, is oriented in such a way that the direction from the source to its drain corresponds to the zigzag direction. The dynamics of electrons and holes in this direction is characterized by a huge effective mass. As a result, a substantial amount of the electrons and holes can relocate from the G-layer (where their mobility could be very high) to the P-layer (with a low mobility).

For the sake of definiteness, we consider the P-layer consisting of several atomic P-layers ($N = 4 - 5$), assuming that in both GP-LD and GP-FET structures it is p-doped (the pristine P-layers are of p-type). At the incident THz photon energies $\hbar\Omega < 2\mu$, where $|\mu|$ is the Fermi energy of the main carriers (holes), the carrier heating is associated with its interband (Drude) absorption in the G-layer.

The band gap Δ_G and the energy spacing Δ^e and Δ^h , between the Dirac point in the G-layer and the edges of the conduction and valence bands, (determined by the pertinent work functions) depend on the number N . In the G-P channel under consideration (with $N = 4$ or 5), the band structure is asymmetric: $\Delta^e > \Delta^h = \Delta$ [14].

The dispersion relation for the holes in the G- and P-layers can be presented as

$$\varepsilon_G^e = v_W \sqrt{p_x^2 + p_y^2}, \quad \varepsilon_P^e = \Delta^e + \frac{p_x^2}{2m_{xx}} + \frac{p_y^2}{2m_{yy}}, \quad (1)$$

$$\varepsilon_G^h = -v_W \sqrt{p_x^2 + p_y^2}, \quad \varepsilon_P^h = -\Delta^h - \frac{p_x^2}{2m_{xx}} - \frac{p_y^2}{2m_{yy}}, \quad (2)$$

respectively. Here $v_W \simeq 10^8$ cm/s is the characteristic velocity of electrons in the G-layers, $m_{xx} = M$ and $m_{yy} = m$ are the components of the effective mass tensor ($M \gg m$), p_x and p_y are the carrier momenta in the source-drain direction and the perpendicular direction, respectively. The components of the effective mass tensor for the valence bands ($N = 4 - 5$) are approximately

equal to $m \simeq 0.04m_0$ and $M \simeq 1.01m_0$, where m_0 is the mass of a free electron.

The model under consideration is based on the following assumptions:

(1) The sufficiently frequent electron-electron, electron-hole, and hole-hole collisions enable the establishment of the distinct quasi-Fermi electron and hole distributions with the common effective temperature T in both G- and P-layers and split quasi-Fermi levels due to the carrier-phonon interband scattering. This is consistent with the numerous experimental studies in which the G-layer was excited with an optical or infrared pump pulse and probed with photoelectron or optical spectroscopy at different photon energies (see, for example, [18] and the references therein). Sufficiently strong interactions between the electrons and holes belonging to both G- and P-layers promote the inter-layer equilibrium [22–24]. Hence, the electron and hole distribution functions are the following functions of the carrier energy ε : $f^{e,h} = [\exp(\varepsilon - \mu^{e,h})/T + 1]^{-1}$ (where μ^e and $\mu^h = \mu$ are the quasi-Fermi energies counted from the Dirac point).

(2) Due to heavy electron and hole effective masses M and \sqrt{mM} , the conductivity of the P-layer is relatively small because this layer mobility in the direction corresponding to the mass M is proportional to $1/\sqrt{mMM}$ [25], so that the P-layer conductivity could be neglected in comparison with the G-layer conductivity. Thus, the main role of the carrier relocation from the G-layer into the P-layer is associated with an intensification of the carriers (in the G-layer) scattering on the carriers (in the P-layer) when the concentration of the latter increases with the carrier system heating.

(3) The momentum relaxation of the electrons and holes in the G-layer (which we refer to as the "light" electrons and holes) is due to their scattering on acoustic phonons, neutral defects, and heavy particles in the P-layer. In contrast to the G-channel-based THz bolometers intended for the operation at very low temperatures at which the carrier energy relaxation is due to the interaction with acoustic phonons, the energy relaxation in the uncooled bolometric detectors under consideration is associated with the optical phonons in the G-layer. The interband transitions assisted by the optical phonons [26, 27] and with the Auger processes (see [28, 29] and the discussion therein) are assumed to be the main recombination-generation mechanisms. We characterize the relative role of these processes by the parameter $\eta = \tau_{Auger}/(\tau_{Auger} + \tau_0^{inter})$, where τ_{Auger} and τ_0^{inter} are the times characterizing the pertinent interband transitions (we call this parameter as the Auger parameter). When $\eta \simeq 1$, the quasi-Fermi energies can be markedly different ($\mu^e \neq -\mu^h$).

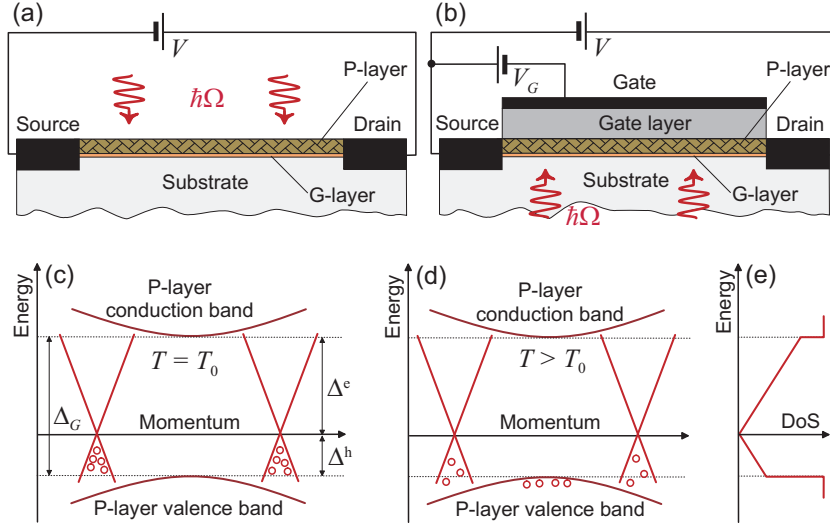


FIG. 1: The structures of (a) the GP-LD and (b) the GP-FET (b), their asymmetric with respect to the Dirac point ($\Delta^e > \Delta^h$) energy band diagrams with the G-Dirac cones and the parabolic extrema corresponding to the P-layer at (c) $T = T_0$ and (d) $T > T_0$, and (e) the energy dependence of the density of state (DoS). Open circles correspond to the holes in the valence bands of G- and P-layers.

III. CONDUCTIVITY OF THE G-P-CHANNEL

The net surface charge density in the GP-channel, which comprises the electron and hole charges in both the G- and P-layers, induced by the acceptors and the gate voltage V_G is equal to $e\Sigma = \kappa|V_G - V_A|/4\pi W_g$ (where $V_G = V_A > 0$, which is proportional to the acceptor density, corresponds to the charge neutrality point, κ and W_g are the background dielectric constant and the thickness of the gate layer, and e is the electron charge). By introducing the voltage (gate) swing $V_g = V_G - V_A$, we unify the consideration of the GP-LDs and GP-FETs. In particular, the case of GP-LDs corresponds to $V_G = 0$, so that $V_g = -V_A < 0$, while in the GP-FETs V_g can be both negative and positive.

The gate voltage swing $V_g = V_G - V_A$ or its dimensional value $U_g = V_g/V_0$ and the quantities T , μ^e , and μ^h are related to each other as

$$U_g = \left(\frac{T}{T_0}\right)^2 \left[\mathcal{F}_1\left(\frac{\mu^e}{T}\right) - \mathcal{F}_1\left(\frac{\mu^h}{T}\right) \right] - \gamma_N \frac{T}{T_0} \ln \left[1 + \exp\left(\frac{\mu^h - \Delta}{T}\right) \right]. \quad (3)$$

Here $\mathcal{F}_1(a) = \int_0^\infty d\xi \xi [\exp(\xi - a) + 1]^{-1}$ is the Fermi-Dirac integral [30], $U_g = (V_G - V_A)/V_0 = V_G/V_0 - \pi\Sigma_A \hbar^2 v_W^2 / 2T_0^2$, $V_0 = 8eT_0^2 W_g / \kappa \hbar^2 v_W^2$, $\gamma_N = N\sqrt{mM}v_W^2 / 2T_0$, and \hbar is the Planck constant. For $N = 5$ and therefore setting $(\sqrt{mM} \simeq 0.2m_0$ and $M/m \simeq 25)$, $W_g = 10 - 1000$ nm and $\kappa = 4$, and $T = 25$ meV ($\simeq 300$ K), one can obtain $\gamma_N \simeq 110$ and $V_0 \simeq 0.05 - 4.94$ V. A large value of γ_N is due to a relatively high density of states in the P-layer.

In equilibrium at sufficiently low temperatures, when

the P-layer is empty (the second term in the right-hand side of Eq. (3) is negligible), Eq. (3) yields $\mu^e = -\mu^h = -\mu \simeq -\hbar v_W \sqrt{\kappa|V_g|/4eW_g}$ when $|V_g|$ is relatively large.

When the electron-hole system in the G-P channel is heated by the source-to-drain DC voltage or by the incident radiation, the electron and hole quasi-Fermi levels can be split: $\mu^e \neq -\mu^h$. Accounting for the competition between the optical phonon mediated and the Auger generation-recombination processes, the equation governing the carrier interband balance can result in the following equation relating μ^e and μ^h at an arbitrary effective temperature T :

$$\mu^e + \mu^h = \eta \hbar \omega_0 \left(1 - \frac{T}{T_0} \right). \quad (4)$$

where $\hbar \omega_0$ is the optical phonon energy. Equation (4) generalizes that obtained previously [13] for the case of the dominant optical phonon generation-recombination processes by the introduction of a phenomenological factor $\eta = \tau_{Auger}/(\tau_{Auger} + \tau_{Opt})$.

Considering Eq. (4), we rewrite Eq. (3) as

$$U_g = \left(\frac{T}{T_0}\right)^2 \left[\mathcal{F}_1\left(-\frac{\mu}{T} - \eta \hbar \omega_0 \left(\frac{1}{T_0} - \frac{1}{T}\right)\right) - \mathcal{F}_1\left(\frac{\mu}{T}\right) \right] - \gamma_N \frac{T}{T_0} \ln \left[1 + \exp\left(\frac{\mu - \Delta}{T}\right) \right]. \quad (5)$$

In particular, using Eq. (5), one can obtain immediately the dependence of the hole Fermi energy $\mu_0 = \mu|_{T=T_0}$ on the voltage swing U_g .

Focusing on the GP-channels with dominant carrier scattering on acoustic phonons, neutral defects, on each

other, and on the short-range screened heavy carriers, the momentum relaxation time $\tau(p)$ as a function of the carrier momentum p can be set as $\tau_p = \tau_0(T_0/pv_W)[\Sigma_G/(\Sigma_G + \Sigma_P)]$, where $\tau_0 \propto \Sigma_G^{-1}$ is the momentum relaxation time in the G-layer with the effective scatterer density Σ_G at $T = T_0$ and $(\Sigma_G + \Sigma_P)$ is the net scatterer density, which accounts for the density, Σ_P , of the heavy carriers in the P-layer. In this case, the GP-channel conductivity could be presented as (in line with [15, 16, 31–36]):

$$\sigma_{GP} = -\frac{\sigma_0 \Sigma_G}{(\Sigma_G + \Sigma_P)} \int_0^\infty d\xi \frac{d(f^e + f^h)}{d\xi} \quad (6)$$

with $\sigma_0 = (e^2 T_0 \tau_0 / \pi \hbar^2)$ being the G-layer low electric-field conductivity. Using Eqs. (4) and (6), the GP-channel conductivity can be expressed via the G-layer conductivity σ_G (without the P-layer conductivity) with the latter expressed via the effective temperature T and the hole quasi-Fermi energy $\mu = \mu^h$:

$$\sigma_{GP} = \frac{\sigma_G \Sigma_G}{(\Sigma_G + \Sigma_P)}, \quad (7)$$

$$\sigma_G = \sigma_0 \left[\frac{1}{\exp\left(\frac{\mu}{T} + \eta \hbar \omega_0 \left(\frac{1}{T_0} - \frac{1}{T}\right)\right) + 1} + \frac{1}{\exp\left(-\frac{\mu}{T}\right) + 1} \right]. \quad (8)$$

The density of scatterers (heavy holes), Σ_P , in the P-layer, which exponentially increases with increasing $|\mu|$ and T , can also be expressed via these quantities:

$$\Sigma_P = \Sigma_N \frac{T}{T_0} \ln \left[1 + \exp\left(\frac{\mu - \Delta}{T}\right) \right], \quad (9)$$

where $\Sigma_N = N T_0 \sqrt{mM} / \pi \hbar^2 \propto \gamma_N$. The factor N in the latter formula reflects the fact that the density of states in the few-layer P-layer increases with the layer number N [15].

The second factor in the right-hand side of Eq. (6) reflects an increase in the scatterer density associated with the inclusion of the scattering on the heavy holes in the P-layer. It is instructive that at $\eta = 0$ when $\mu^e = -\mu^h = -\mu$, the G-channel conductivity $\sigma_G = \sigma_0$ is independent of T . This is because of the specific of the carrier scattering in the system under consideration (scattering on acoustic phonons, neutral defects and effectively screened charged scatterers) [35–38].

Using Eqs. (7) - (9), we obtain

$$\begin{aligned} \sigma_{GP} &= \frac{\sigma_G}{1 + \frac{\Sigma_N T}{\Sigma_G T_0} \ln \left[1 + \exp\left(\frac{\mu - \Delta}{T}\right) \right]} \\ &= \frac{\sigma_0}{1 + \frac{\Sigma_N T}{\Sigma_G T_0} \ln \left[1 + \exp\left(\frac{\mu - \Delta}{T}\right) \right]} \\ &\times \left[\frac{1}{\exp\left(\frac{\mu}{T} + \eta \hbar \omega_0 \left(\frac{1}{T_0} - \frac{1}{T}\right)\right) + 1} + \frac{1}{\exp\left(-\frac{\mu}{T}\right) + 1} \right] \end{aligned} \quad (10)$$

Equations (5) and (10) describe the dependences of the quasi-Fermi energy μ and the G-P-channel conductivity σ_{GP} on the effective temperature T and the voltage swing U_g . Solving these equations, one can obtain the characteristics of the GP-channel in wide ranges of the normalized voltage swing U_g , carrier effective temperature T , and the density Σ_G .

IV. NEGATIVE PHOTOCONDUCTIVITY IN THE G-P CHANNELS

The variation of the current density, $J - J_0$, in the GP-channel for small effective carrier temperature variations is given by

$$J - J_0 \simeq E_{SD} \frac{d\sigma_{GP}}{dT} \Big|_{T=T_0} \cdot (T - T_0), \quad (11)$$

where J_0 is the linear density of the source-drain dc current in the absence of the irradiation (i.e., the dark current density, $E_{SD} = V_{SD}/L$ and V_{SD} are the source-drain electric field and voltage, respectively, L is the length of the GP-channel, and σ_{GP} is given by Eq. (10). An increase in the carrier effective temperature T (the carrier heating) caused by the irradiation corresponds to the negative photoconductivity temperature when the conductivity derivative $(d\sigma_{GP}/dT)|_{T=T_0} < 0$. The latter is in line with the experimental observations [18, 19, 37, 38]. Figure 2 shows $\Lambda_{GP} = \frac{1}{\sigma_0} \frac{d\sigma_{GP}}{d \ln T} \Big|_{T=T_0}$ and

$\Lambda_G = \frac{1}{\sigma_0} \frac{d\sigma_G}{d \ln T} \Big|_{T=T_0}$ (i.e., with $N = 0$) found as functions of U_g using Eqs. (5) and (10) for different values of the scatterer density Σ_G in the G-layer. One can see from Fig. 2 that both the quantities Λ_{GP} and Λ_G are negative. Here and in the following, we assume that $\hbar \omega_0 = 200$ meV, $\Delta = 200$ meV, $\Sigma_N = 1.2 \times 10^{13}$ cm $^{-2}$, $\Sigma_G = 5 \times (10^{10} - 10^{11})$ cm $^{-2}$ corresponding to $\tau_0 = (0.24 - 2.4)$ ps, $\eta = 0.1 - 0.9$, $T_0 = 25$ meV ($\simeq 300$ K), and $\gamma_N = 110$. The scatterer densities range $\Sigma_G = 5 \times (10^{10} - 10^{11})$ cm $^{-2}$ at $\mu_0 = 75$ meV, corresponds to the rather practical values of the carrier mobility in G-layers $b_G \simeq (30 - 300) \times 10^3$ cm 2 /s V [39–42].

At small $|U_g|$, the absolute values of these quantities $|\Lambda_{GP}| \gtrsim |\Lambda_G|$. However, at sufficiently large $|U_g|$, $|\Lambda_{GP}|$

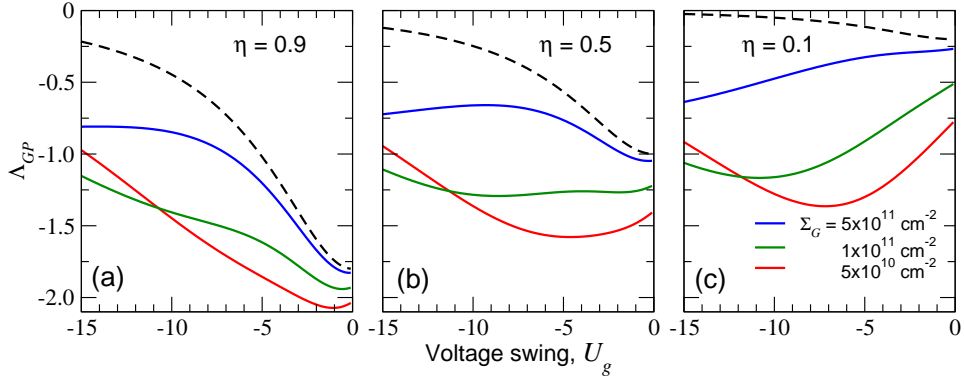


FIG. 2: The temperature derivative of the GP-channel conductivity, Λ_{GP} , versus U_g for $\Delta = 200$ meV and different scatterer densities Σ_G at (a) $\eta = 0.9$, (b) $\eta = 0.5$, and (c) $\eta = 0.1$. Dashed line corresponds to Λ_G ($N = 0$, i.e., $\Sigma_N = 0$) and the same values of η .

can be substantially larger than $|\Lambda_G|$, particularly, at $\eta \ll 1$. This is attributed to a steeper effective temperature dependence of the GP-channel conductivity due to an increasing hole population in the P-layer. The latter implies that the GP-channel can exhibit a stronger temperature dependence and, hence, a stronger effect of the negative photoconductivity than the G-channel. The comparison of the plots in Figs. 2(a) – 2(c) demonstrates that the relative intensification of the Auger processes (a decrease in the parameter η) leads to a marked decrease in $|\Lambda_G|$, diminishing the temperature dependence of the G-channel, while these processes weakly affect the temperature dependence of the GP-channel and, hence, the quantities $|\Lambda_{GP}|$ and $J - J_0$.

V. RESPONSIVITY OF THE GP-PHOTODETECTORS

We limit our following consideration by the GP photodetectors operating as hot-carrier bolometers, so that the incident radiation does not produce a marked amount of the extra electrons and holes and the variation of the carrier density is associated primarily with the heating processes. This happens when $|U_g|$ is sufficiently large (to provide large hole Fermi energy μ), the photon energy $\hbar\Omega$ is not too large ($\hbar\Omega < 2\mu_0$), and the carrier momentum relaxation time τ_0 is not too short, so that the intraband absorption dominates the interband absorption (see Appendix A).

Under irradiation, the carrier effective temperature varies. Its value can be found considering the balance of the power, S_{abs} , receiving by the carriers due to the absorption of the incident radiation with the photon energy $\hbar\Omega$ and the power, $S_{lattice}$, which the carriers transfer to the lattice. As assumed above, the latter is associated with the interband transitions accompanied by the emission and absorption of the G-channel optical phonons having the energy $\hbar\omega_0$. The power received by the carrier system is given by

$$S_{abs} = \frac{4\pi\sigma_{GP}}{c\sqrt{\kappa}} \hbar\Omega I_\Omega = \frac{4\pi}{c\sqrt{\kappa}} \frac{\sigma_{GP}}{(1 + \Omega^2\tau^2)} \hbar\Omega I_\Omega. \quad (12)$$

where c is the speed of light, I_Ω is the radiation photon flux, $\sigma_{GP,\Omega} = \sigma_{GP}/(1 + \Omega^2\tau^2)$ is the high-frequency G-P channel conductivity, τ is the average hole momentum relaxation time in the GP-channel, which considering that $\tau_p \propto 1/p$, can be estimated as

$$\tau \simeq \frac{1}{[2\{\mathcal{F}_1(\mu_0/T_0) + \mathcal{F}_1(-\mu_0/T_0)\}]^{1/2}} \frac{\tau_0}{(1 + P_N)}. \quad (13)$$

Here $P_N = (\Sigma_N/\Sigma_G) \ln\{1 + \exp[-(\Delta - \mu_0)/T_0]\}$. At $\mu_0 \lesssim T_0$ and $\mu_0 \gg T_0$, Eq. (13) yields $\tau \simeq [\sqrt{3}\tau_0/\pi(1 + P_N)]$ and $\tau \simeq [\tau_0/(1 + P_N)](T_0/\mu_0) \simeq \tau_0/\sqrt{2U_g}$, respectively.

Taking into account Eqs. (7), (10), and (12) at $T = T_0$, we obtain

$$S_{abs} = \left(\frac{4\pi\sigma_0}{c\sqrt{\kappa}}\right) \frac{\hbar\Omega I_\Omega}{(1 + P_N)} \frac{1}{(1 + \Omega^2\tau^2)}, \quad (14)$$

As previously [17, 27], we set

$$S_{lattice} = \hbar\omega_0 \frac{\Sigma_0}{\tau_0^{intra}} \left[(\mathcal{N}_0 + 1) \exp\left(-\frac{\hbar\omega_0}{T}\right) - \mathcal{N}_0 \right] \quad (15)$$

where $\mathcal{N}_0 \simeq \exp(-\hbar\omega_0/T_0)$ is the equilibrium number of optical phonons, τ_0^{inter} is the characteristic time of the spontaneous emission of optical phonons at the intraband transitions, and $\Sigma_0 \simeq \pi T_0^2/3\hbar^2 v_W^2$ (at $\mu_0 \lesssim T_0$ and $\Sigma_0 \simeq \mu_0^2/\pi\hbar^2 v_W^2$ (at $\mu_0 \gg T_0$) are the carrier densities in the G-channel at $T = T_0$. For simplicity, below we use the following interpolation formulas:

$$\tau = \frac{\tau_0}{(1 + P_N)} \sqrt{\frac{3}{\pi^2 \left(1 + \frac{6|U_g|}{\pi^2}\right)}}, \quad (16)$$

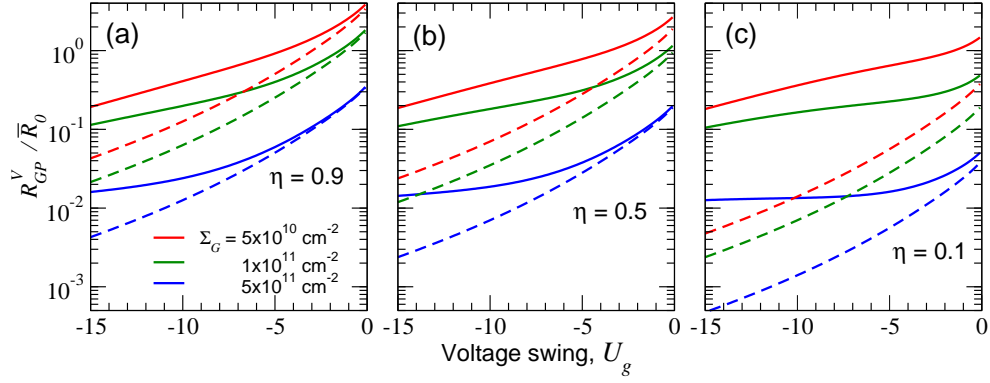


FIG. 3: The normalized GP-bolometer voltage responsivity R_{GP}^V/\bar{R}_0^V versus the voltage swing U_g for the same parameters as in Fig. 2: (a) $\eta = 0.9$, (b) $\eta = 0.5$, and (b) $\eta = 0.1$. Dashed lines correspond to the G-bolometers with the same parameters of the G-layer.

$$\Sigma_0 = \frac{\pi T_0^2}{3\hbar^2 v_W^2} \left(1 + \frac{6|U_g|}{\pi^2} \right). \quad (17)$$

Equalizing S_{abs} and $S_{lattice}$ given by Eqs. (14) and (15), and taking into account Eq. (16), we arrive at the following equation which relates the variation of the carrier effective temperature $T - T_0$ and the photon flux I_Ω :

$$\frac{T - T_0}{T_0} = \left(\frac{12\alpha\hbar v_W^2 \tau_0 \tau_0^\varepsilon}{\pi \sqrt{\kappa} T_0^2} \right) \times \frac{\hbar\Omega I_\Omega}{(1 + P_N)(1 + 6|U_g|/\pi^2)(1 + \Omega^2\tau^2)}, \quad (18)$$

where $\alpha = e^2/c\hbar \simeq 1/137$ is the fine structure constant. The latter formula corresponds to the hole energy relaxation time $\tau_0^\varepsilon = \tau_0^{intra}(T_0/\hbar\omega_0)^2 \exp(\hbar\omega_0/T_0)$. Setting $\tau_0^{intra} = 0.7$ ps (for example, [43]), one obtains $\tau_0^\varepsilon \simeq 32.6$ ps.

Taking into account the variation of the current density, $J - J_0$, in the GP-channel caused by the irradiation, the GP bolometer intrinsic current responsivity R_{GP} can be presented by the following expression:

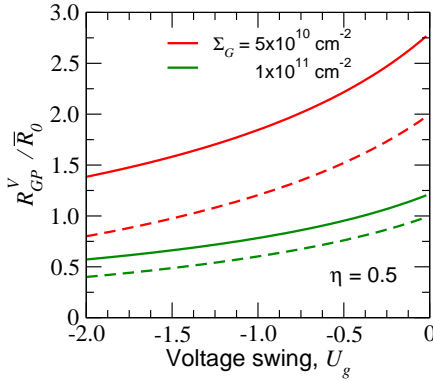


FIG. 4: Zoom of the same plots as in Fig. 3(b).

$$R_{GP} = \frac{(J - J_0)H}{\hbar\Omega I_\Omega A}. \quad (19)$$

Here $A = LH$ is the GP-channel area, L is the channel length (the spacing between the source and the drain), and H is the channel width, i.e., its size in the direction perpendicular to the current direction. Using Eqs. (11) and (18), we arrive at the following:

$$R_{GP} = R_0 \frac{|\Lambda_{GP}|}{[(1 + P_N)(1 + 6|U_g|/\pi^2)(1 + \Omega^2\tau^2)]} \quad (20)$$

Here

$$R_0 = \frac{12\alpha}{\pi^2 \sqrt{\kappa}} \frac{e}{T_0} \frac{ev_W^2 \tau_0^2 \tau_0^\varepsilon E_{SD}}{\hbar L} \propto \tau_0^2, \quad (21)$$

In the above calculations we have not accounted for the carrier heating by the source-drain electric field assuming that it is weak, so that T is very close to T_0 . The pertinent condition is as follows:

$$E_{SD} \ll \bar{E}_{SD} = \frac{\pi T_0}{ev_W} \sqrt{\frac{(1 + P_N)(1 + 6|U_g|/\pi^2)}{3\tau_0 \tau_0^\varepsilon}} = \bar{E}_{SD}^* \sqrt{\frac{(1 + P_N)(1 + 6|U_g|/\pi^2)}{3}}. \quad (22)$$

For $E_{SD} = \bar{E}_{SD}^* = (\pi T_0/ev_W \sqrt{\tau_0 \tau_0^\varepsilon})$, the quantity R_0 , given by Eq. (21), is equal to

$$\max R_0 = \frac{12\alpha}{\pi \sqrt{\kappa}} \frac{v_W \tau_0^{3/2} \sqrt{\tau_0^\varepsilon}}{\hbar L} \propto \tau_0^{3/2}. \quad (23)$$

At $\tau_0 = (0.24 - 2.4)$ ps, $\tau_0^\varepsilon = 32.6$ ps, and $L = 10^{-3}$ cm, for the quantities \bar{E}_{SD}^* and $\max R_0$ one can find $\bar{E}_{SD}^* \simeq (92 - 290)$ V/cm and $\max R_0 \simeq (1.5 - 43.3)$ A/W, respectively.

The voltage responsivity $R_{GP}^V = Rr_L$, where r_L is the load resistance. Setting r_L equal to the GP-channel resistance, i.e., $r_L = L(1 + P_N)/H\sigma_0$. In this case, for R_{GP}^V one obtains

$$R_{GP}^V = R_0^V \frac{|\Lambda_{GP}|}{[(1 + 6|U_g|/\pi^2)(1 + \Omega^2\tau^2)]} \quad (24)$$

with

$$R_0^V = \frac{12\alpha}{\pi\sqrt{\kappa}} \frac{\hbar v_W^2 \tau_0 \tau_0^\varepsilon E_{SD}}{T_0^2 H} \propto \tau_0. \quad (25)$$

Setting $E_{SD} = \overline{E^*}_{SD}$, we arrive at the following expression for the characteristic value of the GP bolometer voltage responsivity:

$$\max R_0^V = \frac{12\alpha}{\sqrt{\kappa}} \sqrt{\tau_0 \tau_0^\varepsilon} \left(\frac{\hbar v_W}{eT_0 H} \right). \quad (26)$$

For $\tau_0 = 0.24 - 2.4$ ps, $\tau_0^\varepsilon = 32.6$ ps, and $H = 10^{-2}$ cm, we obtain $\max R_0^V \simeq (1.85 - 5.85) \times 10^2$ V/W. Naturally, at weaker source-drain electric fields $E_{SD} < \overline{E^*}_{SD} \sim \overline{E}_{SD}$, the quantities R_0 and R_0^V are smaller than $\max R_0$ and $\max R_0^V$.

Using Eqs. (20) and (24) at relatively low frequencies Ω , the current and voltage responsivities can be presented as

$$R_{GP} = \frac{R_0 |\Lambda_{GP}|}{(1 + P_N)(1 + 6|U_g|/\pi^2)}, \quad R_{GP}^V = \frac{R_0^V |\Lambda_{GP}|}{(1 + 6|U_g|/\pi^2)}. \quad (27)$$

Figures 3 and 4 show the GP-bolometers voltage low-frequency responsivity R_{GP}^V normalized by the quantity $\overline{R}_0^V = R_0^V \Big|_{\tau_0=1.2ps}$ as a function of the voltage swing U_g calculated using Eqs. (10) and (27) for the same structural parameters as for Fig. 3 (given in Sec. 4). The normalized responsivity of the G-detectors (with the G-channel) is also shown by the dashed lines. First, as seen from Figs. 3 and 4, the responsivity sharply decreases with an increase in the scatterer density Σ_G and the voltage swing U_g . This is attributed to a weaker carrier heating at their stronger scattering and their larger density. The latter markedly rises with increasing U_g . Second, the GP-bolometer responsivity, moderately exceeding that of the G-bolometer responsivity at small $|U_g|$, becomes orders of magnitudes larger at elevated values of $|U_g|$ (compare the solid and dashed lines in Figs. 3 and 4). The difference in the GP- and G-bolometers responsivities becomes fairly pronounced at smaller Auger parameter η (at stronger Auger generation-recombination processes). This correlates with a drop of Λ_G clearly seen in Fig. 2.

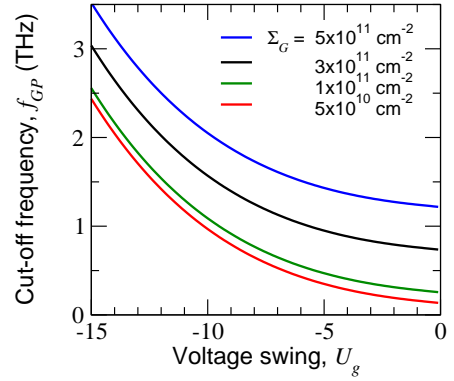


FIG. 5: The cut-off frequency f_{GP} versus the voltage swing U_g for different scatterer densities Σ_G .

VI. BANDWIDTH AND GAIN-BANDWIDTH PRODUCT

As follows from Eqs. (20) and (24), the GP-bolometer responsivity decreases when the photon frequency $\Omega > 2\pi f_{GP}$, where the cut-off frequency is given by

$$\begin{aligned} f_{GP} &= \frac{(1 + P_N)}{2\sqrt{3}\tau_0} \sqrt{\left(1 + \frac{6|U_g|}{\pi^2}\right)} \\ &\simeq \frac{1}{2\sqrt{3}\tau_0} \left[1 + \left(\frac{\Sigma_N}{\Sigma_G}\right) \exp\left(\sqrt{2U_g} - \frac{\Delta}{T_0}\right) \right] \\ &\quad \times \sqrt{\left(1 + \frac{6|U_g|}{\pi^2}\right)}. \quad (28) \end{aligned}$$

At small $|U_g|$, Eq. (27) yields $f_{GP} \simeq (1/2\sqrt{3}\pi\tau_0)$, so that for the values of τ_0 used above, one obtains $f_{GP} \simeq 0.12 - 1.2$ THz. At relatively large $|U_g|$, the frequency $f_{GP} \simeq (1 + P_N)\sqrt{2|U_g|}/2\pi$ can be much higher than that at $U_g \simeq 0$. This is seen from Fig. 5, which shows the cut-off frequency f_{GP} as a function of the normalized voltage swing calculated using Eq. (28). The cut-off frequency f_{GP} is larger than the pertinent frequency for the G-bolometers f_G by a factor $(1 + P_N)$. At large values of Σ_N/Σ_G and U_g , this factor can be larger than that at $U_g \simeq 0$.

The comparison of the gain-bandwidth products of the GP- and G-bolometers, defined as $\max R_{GP}^V f_{GP}$ and $R_G^V f_G$, yields the following estimate for these factors ratio $K \simeq \Lambda_{GP}\Lambda_G$. As seen from Fig. 3, K markedly exceeds unity, particularly at $\eta \ll 1$.

VII. DETECTIVITY OF THE GP-BOLOMETERS

The dark-current-limited detectivity of the GP-bolometers D_{GP}^* can be evaluated as (see, for exam-

ple, [44]:

$$D_{GP}^* = \frac{R_{GP}}{\sqrt{4eJ_0H/A}}. \quad (29)$$

where J_0H is the net source-drain dc current

Equations (18) and (24) for relatively low frequencies Ω yield

$$D_{GP}^* = D_0^* \frac{|\Lambda_{GP}|}{\sqrt{(1+P_N)(1+6|U_g|/\pi^2)}} \quad (30)$$

with

$$D_0^* = \frac{6\alpha}{\pi^{3/2}\sqrt{\kappa}} \frac{v_W^2 \tau_0^{3/2} \tau_0^\varepsilon}{T_0} \sqrt{\frac{eE_{SD}}{LT_0}} \propto \tau_0^{3/2}. \quad (31)$$

for an arbitrary E_{SD} , and

$$\max D_0^* = \frac{6\alpha}{\pi\sqrt{\kappa}} \frac{v_W^{3/2} \tau_0^{5/4} (\tau_0^\varepsilon)^{3/4}}{T_0 L^{1/2}} \quad (32)$$

for $E_{SD} = \overline{E}_{SD}^*$. Using the same parameters as for the above estimates of $\max R_0^V$ and assuming that $L = 10^{-3}$ cm, at $E_{SD} = \overline{E}_{GP}^*$, one obtains $D_0^* \simeq (0.122 - 2.17) \times 10^9$ cm \sqrt{Hz}/W .

The GP-bolometer dark-current-limited detectivity D_{GP}^* , given by Eq. (30), exhibits a fairly steep drop with increasing U_g resembling that of the responsivity R_{GP}^V shown in Fig. 3. One should note that the difference in the detectivities for a smaller Σ_G and those corresponding to a larger Σ_G is more pronounced than the pertinent difference in the responsivities.

VIII. DISCUSSION

A. General comments

As seen from Eq. (11), the quantity $\Lambda_{GB} = \frac{1}{\sigma_0} \left. \frac{d\Sigma_{GP}}{d \ln T} \right|_{T=T_0}$ determines the variation of the GP-channel conductivity due to the carrier heating. Its absolute value $|\Lambda_{GP}|$ exhibits a maximum at a certain value of U_g , which depends on Σ_G . This is seen from Fig. 3. Considering only the variation of the channel conductivity associated with the carrier transfer to the P-layer, from Eq. (10) we find for Λ_{GP} and the maximum of its modulus $|\Lambda_{GP}|^{max}$

$$\Lambda_{GP} \simeq -\frac{P_N}{(1+P_N)^2} \left(1 + \frac{\Delta}{T_0}\right), \quad (33)$$

$$|\Lambda_{GP}|^{max} \simeq \frac{1}{4} \left(1 + \frac{\Delta}{T_0}\right), \quad (34)$$

respectively. This maximum is reached at $P_N = 1$. i.e., at relatively moderate population of the P-layer ($\Sigma_P = \Sigma_G$) that corresponds to $\mu_0 \simeq \Delta - T_0 \ln(\Sigma_N/\Sigma_G)$ or $U_g = -[\Delta/T_0 - \ln(\Sigma_N/\Sigma_G)]^2 = U_g^{max}$. For $\Sigma_G = 5 \times 10^{10}$, 1×10^{11} , and 5×10^{11} cm $^{-2}$, the pertinent values of U_g are approximately equal to -6, -10, and -23, respectively. The latter is in line with plots in Fig. 2. It is interesting that $\max |\Lambda_{GP}|^{max}$ and $|U_g|$ are a linear and a quadratic functions of Δ , respectively.

The obtained results show that the responsivity and detectivity of the GP-bolometers steeply decrease with increasing voltage swing U_g (see Fig. 3). Thus, it is practical to use the range of relatively small $|U_g|$, although the bandwidth of the GP-bolometers extends with increasing $|U_g|$ as seen from Fig. 5. Thus, there is an opportunity of the voltage control of the cut-off frequency. In the GP-LDs, the minimum value of $|U_g|$ is determined by the acceptor density in the GP-channel, so that this density should be minimized to achieve acceptable characteristics. Apart from easier fabrication, the GP-LDs can exhibit the enhance performance of the whole bolometric photodetector due to a more effective THz radiation input.

As demonstrated above, the characteristics of the GL-LD and GL-FET bolometers under consideration can be markedly different depending on the Auger parameter η . This parameter depends on the substrate material, particularly, on its dielectric constant κ . The calculations [29] predicted the optical phonon recombination time in the G-layers from less than a picosecond to several picoseconds at the carrier densities under consideration above and room temperature. The experimental results of the carrier recombination dynamics in G-layer [45] were interpreted assuming that the interband relaxation is associated with the optical phonon processes rather than the carrier-carrier processes, so that $\tau_{Opt} < \tau_{Auger}$ (and η is close to unity). The recent calculations [29] (as well as the previous one's [46]) showed that an increase in κ leads to a virtually linear increase in τ_{Auger} and, hence, in an increase in η . Although, this increase in τ_{Auger} is not too pronounced - the change in κ from 5 to 25 results in a fourfold rise of τ_{Auger} at room temperature [29]. For example, in the case of GP-LDs with SiO $_2$ and hBN substrates, in which $\kappa \sim 4 - 5$, $\tau_{Auger} \lesssim 1$ ps, whereas in the case of the HfO $_2$ substrate, $\tau_{Auger} \gtrsim 2$ ps. In the GP-FETs, the screening of the carrier interaction by a highly conducting gate can substantially suppress the Auger processes. Indeed, using the data obtained recently [29], one can find that τ_{Auger} being $\tau_{Auger} \simeq 1$ ps at $\kappa = 5$ and the gate layer thickness $W_g = 10 - 15$ nm, becomes $\tau_{Auger} \simeq 6$ ps at $W_g = 2$ nm. One needs to point out that in the case of high- κ substrates, additional recombination channel associated with the substrate polar phonons [47] can promote further increase in η . Setting $\tau_{Opt} = (1 - 3)$ ps, we find that the latter values of τ_{Auger} correspond to $\eta = 0.25 - 0.85$. Hence, the range of the Auger parameter η variations assumed in the above calculations appear to be reasonable.

The values of the GP-detector responsivity demonstrated in Fig. 3 are of the same order of magnitude or can exceed the room temperature responsivity of the proposed and realized THz photodetectors based on different heterostructures [21, 48–59], including those based on the P-channel [7, 60, 61] (although in G-based devices at very low temperatures much higher responsivities have been achieved [20]).

B. Assumptions

The main assumptions of our device model are fairly natural and practical. We disregarded the contribution of the carriers in the P-layer to the net conductivity of the G-P-channel. The pertinent condition can be presented as $\sigma_0 \gtrsim eb_P \Sigma_N \exp[(\Delta - \mu_0)/T_0]$ or $\tau_0 \gtrsim \pi \hbar^2 \Sigma_N \exp[(\Delta - \mu_0)/T_0] b_P / e T_0$ where b_P is the carrier mobility in the P-layer. Assuming that $b_P = 330 - 540 \text{ cm}^2/\text{s V}$ [60] (see also [2]) $\Sigma_N = 1.2 \times 10^{13} \text{ cm}^{-2}$, and $\mu_0 < 100 \text{ meV}$ (i.e., $|U_g| < 25$, see Fig. 2), the above inequalities are valid if $\tau_0 \gg 0.005 \text{ ps}$. The values of τ_0 assumed in our calculations well satisfy this requirement.

(i) Above we estimated the scattering time τ_p and, hence, τ_0 as in [15]: $\tau_p^{-1} = v_S p / \hbar$, so that $\tau_0^{-1} = (v_S / v_W)(T_0 / \hbar)$, where $v_S = (\pi^2 U_S^2 l_S^2 \Sigma_G / 4 \hbar^2 v_W)$, $U_S = e^2 / \kappa l_S$ is the characteristic potential of the scatter, and l_S is the screening length. Setting $l_S = 5 \text{ nm}$ or smaller (see also the estimate for l_S at $\mu_0 = 75 \text{ meV}$ [13] and below), we find $v_S \simeq 2 \times 10^7 \text{ cm/s}$. At $\Sigma_G = 10^{12} \text{ cm}^{-2}$ and $T_0 = 25 \text{ meV}$, the latter yields $\tau_0 \simeq 0.12 \text{ ps}$. For the scattering on the acoustic phonons due to the deformation potential interaction with the longitudinal vibrations at $T_0 = 25 \text{ meV}$, one obtains $v_S(ac) \simeq 8 \times 10^5 \text{ cm/s}$ and $\tau_0^{ac} \simeq 3 \text{ ps}$. The contribution of the hole-hole scattering in the G-layer to its dc and ac conductivity are small (despite substantially non-parabolic hole spectrum [59]). The role of the hole-electron scattering is also small due low electron densities, particularly, at high gate voltages.

(ii) The interband absorption of the incident radiation with the photons with the energies $\hbar\Omega \leq 2\pi\hbar f_{GP} < 2\mu_0$ in the G-layer disregarded in our model, is practically prohibited due to the Pauli blocking. At small values of μ_0 (i.e., small $|U_g|$), this absorption is weak in comparison with the intraband (Drude) absorption if

$$\frac{\pi\alpha}{4} \ll \frac{4\pi\Sigma_{GP}}{c(1 + \Omega^2\tau^2)}. \quad (35)$$

At $\Omega < \tau^{-1} = 2\pi f_{GD}$, inequality (31) implies $\tau_0 > (\pi\hbar/16T_0) \simeq 0.005 \text{ ps}$.

(iii) Considering the features of the DoS (see Fig. 1(e)), the screening length, l_S , of the charges in the GP-channel at low and relatively high voltage swing U_g and $T = T_0$ is given by

$$l_S \lesssim \left\{ \frac{\kappa\hbar^2 v_W^2}{8 \ln 2e^2 T_0}, \quad l_S \lesssim \frac{\kappa\hbar^2 v_W^2}{4e^2 \mu_0} \right\}, \quad (36)$$

respectively Assuming $\kappa = 4$ and setting $\mu_0 < T_0 = 25 \text{ meV}$ and $\mu_0 = 60 \text{ meV}$, from Eq. (32) we obtain $l_S \simeq 3.4 - 7.5 \text{ nm}$. The products of the characteristic carrier wavenumbers $k_T = T_0 / \hbar v_W$ and $k_{\mu_0} = \mu_0 / 4\hbar v_W$ and the pertinent values of l_S are $k_T l_S \lesssim 0.31$ and $k_{\mu_0} l_S \lesssim 0.43$. The latter indicates a rather short range interaction (an effective screening of the charged impurities and the heavy carriers in the P-layer) in the device under consideration at its working conditions.

IX. CONCLUSIONS

We studied the effect of THz photoconductivity of the G- and GP-channels and showed that their conductivity decreases under the THz irradiation (the effect of negative conductivity). It was revealed that this effect in G-channels is determined by the competition of the interband transitions associated with optical phonons and the Auger generation-recombination processes and vanishes when the latter processes prevail. However, the negative conductivity in the GP-channels is weakly sensitive to the relative roles of the latter process. The negative photoconductivity of the ungated and gated GP-channels (GP-LDs and GP-FETs) under the THz irradiation, enables using these devices as bolometric THz photodetectors. We evaluated the responsivity, bandwidth, and detectivity characteristics of such THz bolometers and demonstrated that an effective transfer of the carriers from the G-layer into the P-layer, caused by their heating due to the intraband absorption of the THz radiation, leads to the substantial decrease in the G-P-channel conductivity. This effect of the negative THz photoconductivity is associated primarily with the intensification of the light carrier scattering in the G-layer on the heavy carriers in the P-layer. Using the developed device model for the GP-LD and GP-FET bolometers, we demonstrated that these photodetectors can exhibit a fairly high responsivity in a wide range of the THz frequencies at the room temperature. The main requirement to achieve the elevated photodetector performance is having sufficiently high values of the G-layer mobility. The main characteristics of the GP-FET bolometers are effectively controlled by the gate voltage. The GP-LD and GP-FET THz bolometric photodetectors can substantially surpass the THz bolometers with the G-channel and compete and even outperform the existing devices. Further enhancement of the GP-LD and GP-FET THz bolometer can be realized using the GP-GP-...-GP superlattice heterostructures as the channel, integrating the GP-LDs and GP-FETs with THz microcavities or waveguides, and implementing different schemes of the plasmonic enhancement of the THz absorption.

Appendix A. Short-range versus long-range scattering

As seen from Fig. 2, in the G-channels the quantity $\Lambda_G < 0$. This implies that the carrier heating in the G-layers by the absorbed radiation leads to a decrease in the conductivity, i.e. to the negative photoconductivity. This phenomenon was observed in the experiments (see, for example, [18, 19, 37, 38]). As shown above, the G-layer negative photoconductivity at the room temperatures can appear when the short-range scattering dominates and the Auger generation-recombination processes are weaker than those associated with the optical phonons. In the case of the dominant long-range scattering, the G-layer conductivity rises with increasing carrier effective temperature [15]. In the model [18], the G-layer conductivity was considered assuming that $\tau_p = \tau_0$ is independent of carrier momentum p . In such a model,

$$\begin{aligned} \sigma_G &\propto \int_0^\infty d\xi \xi \frac{d(f^e + f^h)}{d\xi} \\ &= \ln \left[\left(1 + e^{\mu^e/T} \right) \left(1 + e^{\mu^h/T} \right) \right]. \end{aligned} \quad (\text{A1})$$

At small and high ratios μ^e/T and μ^h/T , Eq. (A1) yields $\sigma_G \propto [4 + (\mu^e + \mu^h)/2T]$ and $\sigma_G \propto (\mu^e + \mu^h)/T$, respectively. This results (accounting for Eq. (4)) in $\sigma_G \propto [4 + \eta\hbar\omega(1/T - 1/T_0)]$ and $\sigma_G \propto \eta\hbar\omega(1/T - 1/T_0)$. One can see that at $\tau_p = \text{const}$, as in the case $\tau_p \propto 1/p$ considered by us, the G-layer conductivity decreases with increasing carrier temperature. However, this effect vanishes (the conductivity becomes insensitive to the carrier temperature variation and, hence, to the irradiation) when the Auger parameter η tends to zero. Thus, even in this case, the carrier temperature dependence of the GP-channel conductivity σ_{GP} , related to σ_G according to Eq. (10), corresponds to the negative photoconductivity with the main contribution of the carrier transfer to the P-layer.

On the contrary, if the long-range scattering with $\tau_p \propto p$ would dominate, σ_G could be a rising function of the carrier temperature leading to the positive G-layer photoconductivity. This can surpass the effect of the G-to-P carrier transitions. Both types of the G-layer photoconductivity (negative and positive) depending on the photon energy and the environmental gases have been observed, for example, in [38].

Appendix B. Frequency dependence of the GP- and G-channel conductivity

Following the standard procedures (see, for example, [32]), the ac conductivity can be presented as (com-

pare with Eq. (6))

$$\sigma_{GP,\Omega} = -\frac{\sigma_0 \Sigma_G}{\Sigma_G + \Sigma_P} \int_0^\infty \frac{d\xi [d(f^e + f^h)/d\xi]}{1 + \frac{\Omega^2 \tau_0^2 \Sigma_G^2}{(\Sigma_G + \Sigma_P)^2 \xi^2}}. \quad (\text{B1})$$

At low and high frequencies frequencies, Eq. (B1) can be rewritten as

$$\sigma_{GP,\Omega} \simeq \sigma_{GP} \simeq \frac{\sigma_0 \Sigma_G}{(\Sigma_G + \Sigma_P)}, \quad (\text{B2})$$

$$\sigma_{GP,\Omega} \simeq \frac{\sigma_{GP}}{\Omega^2 \tau^2} \simeq \frac{\sigma_0 \Sigma_G}{(\Sigma_G + \Sigma_P)} \frac{1}{\Omega^2 \tau^2}, \quad (\text{B3})$$

respectively, where

$$\frac{1}{\tau} = \frac{2}{\tau_0} \frac{(\Sigma_G + \Sigma_P)}{\Sigma_G} \left[\mathcal{F}_1 \left(-\frac{\mu_0}{T_0} \right) + \mathcal{F}_1 \left(\frac{\mu_0}{T_0} \right) \right]^{1/2}. \quad (\text{B4})$$

For $U_g \simeq 0$ and $U_g \gg 1$, Eq. (B4) yields

$$\tau \simeq \frac{\sqrt{3}\tau_0}{\pi(1 + P_N)} \quad \tau \simeq \frac{1}{(1 + P_N)\sqrt{2|U_g|}}, \quad (\text{B5})$$

so that τ as a function of $|U_g|$ can, for example, be interpolated by Eq. (16). In the case of the dominating long-range scattering, for the cut-off frequency one obtains $f_{GP} \simeq 1/2\pi\tau_0$.

Acknowledgments

The authors are grateful to P. P. Maltsev, A. Satou, D. Svintsov, and V. Vyurkov for useful discussions. VR is also thankful to N. Ryabova for assistance. his work was supported by Japan Society for Promotion of Science, KAKENHI Grant No. 16H06361, the Russian Science Foundation (Grant No.14-29-00277), Russian Foundation for Basic Research (Grant No. 18-07-01145), RIEC Nation-Wide Collaborative Research Project, and by Office of Naval Research (Project Monitor Dr. Paul Maki).

-
- [1] A. H. Castro Neto, F. Guinea, N. M. R. Peres, K. S. Novoselov, and A. K. Geim, “The electronic properties of graphene,” *Rev. Mod. Phys.* **81** 109–162(2009).
- [2] Xi Ling, H. Wang, S. Huang, F. Xia, and M. S. Dresselhaus, “The renaissance of black phosphorus,” *Proc. Nat. Acad. Sci USA*, **112**, 4523–4530 (2015).
- [3] F. Bonaccorso, Z. Sun, T. Hasan, and A. Ferrari, “Graphene photonics and optoelectronics,” *Nat. Photonics* **4**, 611–622 (2010).
- [4] V. Ryzhii, M. Ryzhii, V. Mitin, and T. Otsuji, “Toward the creation of terahertz graphene injection laser,” *J. Appl. Phys.* **110**, 094503 (2011).
- [5] Q. Bao and K. P. Loh, “Graphene photonics, plasmonics, and broadband optoelectronic devices,” *ACS Nano* **6**, 3677–3677 (2012).
- [6] A. Tredicucci and M. Vitiello, “Device concepts for graphene-based terahertz photonics,” *J. Sel. Top. Quant.* **20**, 130–138 (2014).
- [7] M. Buscema, D. J. Groenendijk, S. I. Blanter, G. A. Steele, H. S. J. van der Zant, and A. Castellanos-Gomez, “Fast and broadband photoresponse of few-layer black phosphorus field-effect transistors,” *Nano Lett.* **14**, 3347–3352 (2014).
- [8] M. Engel, M. Steiner, and Ph. Avouris, “A black phosphorus photo-detector for multispectral high-resolution imaging,” *Nano Lett.* **14**, 6414–6417 (2014).
- [9] E. Leong, R. J. Suess, A. B. Sushkov, H. D. Drew, T. E. Murphy, and M. Mittendorff, “Terahertz photoresponse of black phosphorus,” *Opt. Express* **25**, No. 11, 12666–12674 (2017).
- [10] F. Ahmed, Y. D. Kim, M. S. Choi, X. Liu, D. Qu, Z. Yang, J. Hu, I. P. Herman, J. Hone, W. J. Yoo, “High electric field carrier transport and power dissipation in multilayer black phosphorus field effect transistor with dielectric engineering,” *Adv. Funct. Mater.* **27**, 1604025 (2017).
- [11] Y. Deng, Z. Luo, N. J. Conrad, H. Liu, Y. Gong, S. Najmaei, P. M. Ajayan, J. Lou, X. Xu, P. D. Ye, “Black phosphorus-monolayer MoS₂ van der Waals heterojunction p-n diode,” *ACS Nano* **8**, 8292–8299 (2014).
- [12] F. H. L. Koppens, T. Mueller, Ph. Avouris, A. C. Ferrari, M. S. Vitiello, and M. Polini, “Photodetectors based on graphene, other two-dimensional materials and hybrid systems,” *Nat. Nanotech.* **9**, 780–793 (2014).
- [13] V. Ryzhii, M. Ryzhii, D. Svitsov, V. Leiman, P. P. Maltsev, D. S. Ponomarev, V. Mitin, M. S. Shur, and T. Otsuji, “Real-space-transfer mechanism of negative differential conductivity in gated graphene-phosphorene hybrid structures: Phenomenological heating model,” *J. Appl. Phys.* **124** (2018), in press [arXiv: 1806.06227 (2018)].
- [14] Y. Cai, G. Zhang, and Y.-W. Zhang, “Layer-dependent band alignment and work function of few-layer phosphorene,” *Sci. Reports* **4**, 6677 (2014).
- [15] F. T. Vasko and V. Ryzhii, “Voltage and temperature dependencies of conductivity in gated graphene,” *Phys. Rev. B* **76**, 233404 (2007).
- [16] O. G. Balev, F. T. Vasko, and V. Ryzhii, “Carrier heating in intrinsic graphene by a strong dc electric field” *Phys. Rev. B* **79**, 165432 (2009).
- [17] V. Ryzhii, T. Otsuji, M. Ryzhii, N. Ryabova, S. O. Yurchenko, V. Mitin, and M. S. Shur, “Graphene terahertz uncooled bolometers,” *J. Phys. D: Appl. Phys.* **46**, 065102 (2013).
- [18] J. N. Heyman, J. D. Stein, Z. S. Kaminski, A. R. Banman, A. M. Massari, and J. T. Robinson, “Carrier heating and negative photoconductivity in graphene,” *J. Appl. Phys.* **117**, 015101 (2015).
- [19] Xu Du, D. E. Prober, H. Vora, and C. Mckitterick, “Graphene-based bolometers,” *Graphene 2D Mater.* **1**, 1–22 (2014).
- [20] Qi Han, T. Gao, R. Zhang, Yi Chen, J. Chen, G. Liu, Y. Zhang, Z. Liu, X. Wu, and D. Yu, “Highly sensitive hot electron bolometer based on disordered graphene,” *Sci Rep.* **3**, 3533 (2013).
- [21] G. Skoblin, J. Sun, and A. Yurgens, “Graphene bolometer with thermoelectric readout and capacitive coupling to an antenna,” *Appl. Phys. Lett.* **112**, 063501 (2018)
- [22] G. Zhang, A. Chaves, S. Huang F. Wang1, Q. Xing, T. Low, and H. Yan1, “Determination of layer-dependent exciton binding energies in few-layer black phosphorus,” *Sci. Advances* **16** Mar 2018: Vol. 4, no. 3, eaap9977.
- [23] T. Low, R. Roldn, H. Wang, F. Xia, P. Avouris, L. M. Moreno, F. Guinea, “Plasmons and screening in monolayer and multilayer black phosphorus,” *Phys. Rev. Lett.* **113**, 106802 (2014).
- [24] S. Yuan, A. N. Rudenko, and M. I. Katsnelson, “Transport and optical properties of single- and bilayer black phosphorus with defects,” *Phys. Rev. B* **91**, 115436 (2015).
- [25] J. Xi, M. Long, D. Wang, and Z. Shuai, “First principles prediction of charge mobility in carbon and organic nanomaterials,” *Nanoscale* **4**, 4348–4369 (2012).
- [26] F. Rana, P. A. George, J. H. Strait, S. Sharavaraman, M. Charasheyhar, and M. G. Spencer, “Carrier recombination and generation rates for intravalley and intervalley phonon scattering in graphene,” *Phys. Rev. B* **79**, 115447 (2009).
- [27] V. Ryzhii, M. Ryzhii, V. Mitin, A. Satou, and T. Otsuji, “Effect of heating and cooling of photogenerated electron-hole plasma in optically pumped graphene on population inversion,” *Jpn. J. Appl. Phys.* **50**, 094001 (2011).
- [28] M. S. Foster and I. L. Aleiner, “Slow imbalance relaxation and thermoelectric transport in graphene,” *Phys. Rev. B* **79**, 085415 (2009).
- [29] G. Alymov, V. Vyurkov, V. Ryzhii, A. Satou, and D. Svitsov, “Auger recombination in Dirac materials: A tangle of many-body effects,” *Phys. Rev. B* **97**, 205411 (2018).
- [30] J. S. Blakemore, *Semiconductor Statistics*, Dover, 1987.
- [31] T. Ando, “Screening Effect and impurity scattering in monolayer graphene,” *J. Phys. Soc. Japan* **75**, 074716 (2006)
- [32] L. A. Falkovsky and A. A. Varlamov, “Space-time dispersion of graphene conductivity,” *European Phys. J. B* **56**, 281–284 (2007).
- [33] E. H. Hwang, S. Adam, and S. D. Sarma, “Carrier transport in two-dimensional graphene layers,” *Phys. Rev. Lett.* **98**, 186806 (2007).
- [34] V. Vyurkov and V. Ryzhii, “Effect of Coulomb scattering on graphene conductivity,” *JETP Lett.* **88**, 370–372 (2008).

- [35] E. H. Hwang and S. Das Sarma, “Acoustic phonon scattering limited carrier mobility in two-dimensional extrinsic graphene,” *Phys. Rev. B* **77**, 115449 (2008).
- [36] E. H. Hwang and S. Das Sarma, “Screening induced temperature dependent transport in 2D graphene,” *Phys. Rev. B* **79**, 165404 (2009).
- [37] G. Jnawali, Y. Rao, H. G. Yan, and T. F. Heinz, “Observation of a transient decrease in terahertz conductivity of single-layer graphene induced by ultrafast optical excitation,” *Nano Lett.* **13**, 524–530 (2013).
- [38] C. J. Docherty, C. T. Lin, H. J. Joyce, R. J. Nicholas, L. M. Hertz, L. J. Li, and M. B. Johnston, “Extreme sensitivity of graphene photoconductivity to environmental gases,” *Nat. Comm.* **3**, 1228 (2012).
- [39] S. V. Morozov, K. S. Novoselov, M. I. Katsnelson, F. Schedin, D. C. Elias, J. A. Jaszczak, and A. K. Geim, “Giant intrinsic carrier mobilities in graphene and its bilayer,” *Phys. Rev. Lett.* **100**, 016602 (2008).
- [40] H. Hirai, H. Tsuchiya, Y. Kamakura, N. Mori, and M. Ogawa, “Electron mobility calculation for graphene on substrates,” *J. Appl. Phys.* **116**, 083703 (2014).
- [41] L. Banszerus, M. Schmitz, S. Engels, J. Dauber, M. Oellers, F. Haupt, K. Watanabe, T. Taniguchi, B. Beschoten, and C. Stampfer, “Ultrahigh-mobility graphene devices from chemical vapor deposition on reusable copper,” *Science Advances* **1**, No. 6, e1500222 (2015).
- [42] L. Wang, I. Meric, P. Y. Huang, Q. Gao, Y. Gao, H. Tran, T. Taniguchi, K. Watanabe, L. M. Campos, D. A. Muller, J. Guo, P. Kim, J. Hone, K. L. Shepard, and C. R. Dean, “One-dimensional electrical contact to a two-dimensional material,” *Science* **342**, 614–617 (2013).
- [43] K. J. Tielrooij, J. C.W. Song, S. A. Jensen, A. Centeno, A. Pesquera, A. Z. Elorza, M. Bonn, L. S. Levitov, and F. H.L. Koppens, “Photoexcitation cascade and multiple hot-carrier generation in graphene,” *Nat. Phys.* **9**, 248–252 (2013).
- [44] H. Schneider and H.C, Liu, *Quantum Well Infrared Photodetectors: Physics and Applications*, Springer, NY, 2007.
- [45] J. M. Dawlaty, S. Shivaraman, M. Chandrashekar, F. Rana, and M. G. Spencer “Measurement of ultrafast carrier dynamics in epitaxial graphene,” *Appl. Phys. Lett.* **92**, 042116 (2008).
- [46] F. Rana, “Electron-hole generation and recombination rates for coulomb scattering in graphene,” *Phys. Rev. B* **76**, 155431 (2007).
- [47] F. Rana, J. H. Strait, H. Wang, and C. Manolatu, “Ultrafast carrier recombination and generation rates for plasmon emission and absorption in graphene,” *Phys. Rev. B* **84**, 045437 (2011).
- [48] S. D. Gunapala, S. V. Bandara, J. K. Liu, J. M. Mummolo, S. B. Rafol, D. Z. Ting, A. Soibel, and C. Hill, “Quantum Well Infrared Photodetector Technology and Applications,” *IEEE J. Sel. Topics Quant. Electron.* **20**, No. 6 (2014).
- [49] V. Ryzhii, T. Otsuji, V. E. Karasik, M.Ryzhii, V. Leiman, V. Mitin, and M. S. Shur, “Comparison of intersubband quantum-well and interband graphene layer infrared photodetectors,” *IEEE J. Quant. Electron.* **54**, No. 2 (2018).
- [50] V. Ryzhii, M. Ryzhii, M. S. Shur, V. Mitin, A Satou, and T Otsuji, “Resonant plasmonic terahertz detection in graphene split-gate field-effect transistors with lateral pn junctions,” *J. Phys. D: Appl. Phys.* **49**, 315103 (2016).
- [51] M. Mittendorff, S. Winnerl, J. Kamann, J. Eroms, D. Weiss, H. Schneider, and M. Helm, “Ultrafast graphene-based broadband THz detector,” *Appl. Phys. Lett.* **103**, 021113 (2013).
- [52] V.Ryzhii, M.Ryzhii, D.Svintsov, V.Leiman, V.Mitin, M.S.Shur, and T .Otsuji, “Nonlinear response of infrared photodetectors based on van der Waals heterostructures with graphene layers,” *Optics Express* **25**, 5536–5549 (2017).
- [53] V. Ryzhii, M. Ryzhii, V. Leiman, V. Mitin, M. S. Shur, and T. Otsuji, “Effect of doping on the characteristics of infrared photodetectors based on van der Waals heterostructures with multiple graphene layers,” *J. Appl. Phys.* **122**, 054505 (2017).
- [54] V. Ya. Aleshkin, A. A. Dubinov, S. V. Morozov, M. Ryzhii, T. Otsuji, V. Mitin, M. S. Shur, and V. Ryzhii, “Interband infrared photodetectors based on HgTe-CdHgTe quantum-well heterostructures,” *Opt. Mat. Exp.* **8**, 1349 (2018).
- [55] V. Ryzhii, M. Ryzhii, V. Mitin, and T. Otsuji, “Terahertz and infrared photodetection using p-i-n multiple-graphene-layer structures,” *J. Appl. Phys.* **107**, 054512 (2010).
- [56] A. V. Muraviev, S. L. Rumyantsev, G. Liu, A. A. Balandin, W. Knap, and M. S. Shur, “Plasmonic and bolometric terahertz detection by graphene field-effect transistor,” *Appl. Phys. Lett.* **103**, 181114 (2013)
- [57] Y. Wang, W. Yin, Q. Han, X. Yang, H. Ye, Q. Lv, D. Yin, “Bolometric effect in a waveguide-integrated graphene photodetector,” *Chin Phys. B* **25**, 118103 (2016).
- [58] D. A. Bandurin, D. Svintsov, I. Gayduchenko, S. G. Xu, A. Principi, M. Moskotin, I. Tret'yakov, D. Yagodkin, S. Zhukov, T. Taniguchi, K. Watanabe, I. V. Grigorieva, M. Polini, G. Goltsman, A. K. Geim, and G. Fedorov, “Resonant terahertz detection using graphene plasmons,” *arXiv: 1807.04703* (2018).
- [59] D. S. Ponomarev, D. V. Lavruchin, A. E. Yachmenev, R. A. Khabibullin, I. E. Semenikhin, V. V. Vyurkov, M. Ryzhii, T. Otsuji, and V. Ryzhii, “Lateral terahertz hot-electron bolometer based on an array of Sn nanowires in GaAs,” *J. Phys. D: Appl. Phys.* **51**, 135101 (2018).
- [60] L. Viti, J. Hu, D. Coquillat, A. Politano, W. Knap, and M. S. Vitiello, “Efficient Terahertz detection in black-phosphorus nano-transistors with selective and controllable plasma-wave, bolometric and thermoelectric response,” *Scientific Reports* **6**, 20474 (2016).
- [61] E. Leong, R. J. Suess, A. B. Sushkov, H. D. Drew, T. E. Murphy, and M. Mittendorff, “Terahertz photoresponse of black phosphorus,” *Optics Express* **25**, 12666–12674 (2017).
- [62] D. Svintsov, V. Ryzhii, A. Satou, T. Otsuji, and V. Vyurkov, “Carrier-carrier scattering and negative dynamic conductivity in pumped graphene,” *Optics Express* **22**, 19873–19886 (2014).